High Activity Pd-Fe Bimetallic Catalysts for Aqueous Phase Hydrogenations

Yan Cheng[1,2], Hien Pham[2,3], Jiajie Huo[1,2], Robert Johnson[1,2], Abhaya K. Datye[2,3], Brent Shanks[1,2,*]

1. Department of Chemical & Biological Engineering, Iowa State University, Ames, IA, 50010
2. Center for Biorenewable Chemicals, Iowa State University, Ames, IA, 50010
3. Department of Chemical & Biological Engineering and Center for Microengineered Materials, University of New Mexico, Albuquerque, NM, 87131

* Corresponding author. bshanks@iastate.edu

Abstract

Palladium-iron bimetallic catalysts were synthesized using carbon-coated silica supports that provided high hydrogenation activity relative to monometallic palladium under condensed-phase hydrothermal conditions. The catalysts were applied to the hydrogenation of carbonyl groups in acetone, 2-pentanone, and propionaldehyde. While Fe incorporation independent of Pd-to-Fe ratio gave enhanced activity, the catalysts having more Fe than Pd gave more than a three-fold increase in hydrogenation activity relative to the Pd only counterpart. The activity enhancement appeared to be related to the influence of Fe on the Pd as Fe under the condensed-phase reaction conditions was inert. The catalysts were also tested for hydrogenation of unsaturated carbon-carbon double bond and aromatic rings in which more moderate activity enhancement was observed. Through evaluating the influence of Pd-to-Fe ratio on catalyst properties and catalytic performance for the range of molecules, it is proposed that the turnover frequency enhancement can be attributed to the formation of $Pd^{\delta-}$ via Pd-Fe interaction.

Keywords: condensed-phase hydrogenation, Pd-Fe, bimetallic, carbonyl hydrogenation

1. Introduction

The conversion of biomass to chemicals and fuels commonly introduces the need for hydrogenation catalyst technology relevant to the condensed phase[1]. A significant gap still exists between understanding hydrogenation catalyst activity under condensed phase versus vapor phase conditions. However, an increasing number of catalyst properties including metal particle size[2,3], catalyst morphology[2], metal electronic state[4–6], support effects[7,8] and surface polarity[9] have been examined. In addition to properties associated with monometallic supported catalysts, the incorporation of multi-metals has also been explored to tune catalytic properties as reviewed by several groups[9–12].

Bimetallic catalysts can show distinct performance from that of the respective monometallics due to tuned electronic and chemical properties of the alloy[13] or synergic effects of noncompetitive adsorption[14]. For example, Huber et al. [15] studied the aqueous-phase reforming of ethylene glycol over alumina supported Pd and Pt bimetallic catalysts. They found that Fe promoted Pd gave a turnover frequency (TOF) that was 39-46 times higher than Pd alone. Not only can a secondary metal improve catalyst activity, but the stability of the catalyst against leaching, even in acidic aqueous solutions, as shown by Tang et al.[16] for the oxygen reduction reaction (ORR) can be enhanced. After synthesis of the carbon supported Pd-Fe catalyst, the authors treated the catalyst with sulfuric acid to remove Fe. It was found that the Fe dissolved except those forming alloys with Pd, which suggested the alloyed Fe had high resistance to the acidic aqueous solution. Analysis of the catalyst with EDS and X-ray diffraction were used to suggest that the Pd-Fe particles was partially covered by non-alloying Fe that could be removed by the acid treatment.

Pd-Fe bimetallic catalysts have been reported to be effective in a diverse set of reactions including water-gas shift[17], nitro reduction[18,19], hydrodechlorination[20,21], and hydrogenolysis[12]. In contrast, results for hydrogenation reactions with Pd-Fe bimetallic catalysts have shown differing performance as summarized in Table 1. Higher activity was reported for condensed phase hydrogenation of propionaldehyde, xylose, and furfural[22] and aliphatic aldehydes and ketones[23] and for gas phase hydrogenation of styrene[24] and carbon monoxide[25], while lower activity for the Pd-Fe bimetallic compared to Pd was reported for condensed phase hydrogenation of phenol[26], and 1-hexene[27], and gas phase hydrogenation of 1,3-butadiene[28], and benzo[a]pyrene hydrogenation in supercritical carbon dioxide[29].

The goal of the current work was to more extensively examine the hydrogenation activity of Pd-Fe bimetallic catalysts in condensed phase reactions by testing their performance with multiple molecules containing diverse functional groups including aldehyde, ketone, carbon double bond and aromatic. More extensive hydrogenation testing was performed with acetone to examine the impact of the Pd-to-Fe ratio and longer-term reaction performance of the catalysts.

Catalyst Support	Reactant	Solvent/Phase	Bimetallic Activity [a]	Reference
ferric oxide	aliphatic aldehydes, ketones	ethanol	+	[23]
alumina	styrene	gas	+	[24]

alumina	propionaldehyde, xylose, furfural	water	+	[22]
silica	carbon monoxide	gas	+	[25]
iron powder	benzo[a]pyrene	supercritical carbon dioxide	-	[29]
carbon	1-hexene	n-heptane	-	[27]
alumina	1,3-butadiene	gas	-	[28]
alumina	phenol	water	-	[26]

a. '+' indicates higher activity on Pd-Fe bimetallic compared to Pd monometallic catalysts, while '-' indicates lower activity

Table 1. Hydrogenation reactions studied with Pd-Fe bimetallic catalysts

2. Experimental

2.1 Chemicals

Davisil grade 646 silica gel (150Å, 35-60 mesh), propionaldehyde (≥97%), 2-pentanone (99%), 5-hexen-2-one (99%), phenol (≥ 99.0%), ferrous acetate (95%), palladium (II) acetate (≥99.9%), furfuryl alcohol (98%) were used as purchased from Sigma-Aldrich. Acetone (99.7%), isopropanol (99.9%) and 1,4-dioxane (99%) were purchased from Fisher. Benzene (99.0%) was purchased from Alfa Aesar. Industrial grade hydrogen and nitrogen used in the synthesis as well as ultra-high purity hydrogen used in the hydrogenation reactions were purchased from Airgas.

2.2 Catalysts synthesis and characterization

Prior to use, the Davisil silica was washed with nanopure water until the rinse liquid was clear and then dried at 120^{o}C. The desired amount of furfural alcohol was impregnated on Davisil silica as to form two molecule layers. After drying at 80^{o}C for 3 hours, the furfuryl alcohol impregnated silica was heated to 120^{o}C for 12h to oligomerize the coating. Then, the coated material was put under nitrogen flow in a quartz tube at 800^{o}C (1^{o}C/min) for 10 hours to obtain the final carbon coated silica, which is referred to as the support in this manuscript. Fe and Pd were loaded onto the support by sequential incipient-wetness impregnation, using an aqueous solution of ferrous acetate and an acetone solution of palladium acetate. After drying in an oven at 120^{o}C for 12h, the metal-impregnated support was reduced at 200^{o}C in H_2 flow. The loading of Pd on all catalysts was 1 wt%, while the relative molar concentration of Pd in the Pd-Fe bimetallic was varied from 10%, 20%, 45%, 75%, and 100%, denoted as Pd_{10}, Pd_{20}, Pd_{45}, Pd_{75} and Pd_{100} respectively.

The overall metal loading in the catalysts were analyzed using inductively coupled plasma-optical emission spectroscopy (ICP-OES) with a Perkin Elmer Optima 8000 instrument. Catalysts were dispersed in ethanol and mounted on holey carbon grids for examination in a JEOL 2010F 200 kV transmission electron microscope equipped with an Oxford Energy Dispersive System (EDS) for elemental analysis. The Pd concentration in individual particles was analyzed in high angle annular dark field (HAADF) mode.

Pd dispersion was determined using CO chemisorption with a Micromeritics ASAP 2920 analyzer. The catalyst was first reduced by 50 ml/min 10% H_2-Ar at 200ºC for 1 h. Then 20 ml/min He was introduced to purge the sample at 200ºC for 1 h before the catalyst was cooled to room temperature. The catalyst was heated at a rate of 10ºC/min to 35ºC. After the baseline was stable on the thermal conductivity detector, a series of pulse streams of 10% CO-He was injected onto the catalyst until the injected gas volume emerged from the sample tube unchanged and the detected peaks were constant in area. The stoichiometry factor for CO adsorption was assumed to be 1.

Pd particle size distribution and mean surface diameter were obtained from the high angle annular dark field scanning transmission electron microscopy (HAADF-STEM) images. In addition to analysis in the HAADF mode, bright field HRTEM was performed to identify the phases of the metal nanoparticles by their lattice fringes. The size of each individual particle was measured manually using ImageJ software and the Gauss-averaged diameter were calculated by fitting the data with a Gaussian distribution curve using the software Origin.

To examine the relative bonding strength of hydrogen on the materials, hydrogen temperature programmed desorption (TPD) was performed with a Micromeritics ASAP 2920. The method was adapted from that reported previously[30]. Specifically, 50 mg of catalyst was reduced at 200°C for 1h with a heating rate of 10°C/min under 10% H_2-Ar flow (50 ml/min) and then it was purged with an Ar flow (50 ml/min) for 15 min. After cooling the reduced catalyst to 35°C under Ar flow (50 ml/min), a 10% H_2-Ar mixed gas (50 ml/min) was injected for 60 min at 35°C. The sample was purged under Ar flow (50 ml/min) to remove physisorbed hydrogen, and subsequently the furnace temperature was increased from 35°C to 200°C at a heating rate of 10°C/min under Ar flow (50 ml/min) and held at 200°C for 30 minutes. The desorbed hydrogen was detected using a thermal conductivity detector (TCD). The data reported were smoothed using a MATLAB 'rlowess' method with span of 10% of the data points.

X-ray powder diffraction (XRD) and x-ray photoelectron spectroscopy (XPS) were performed in an attempt to understand the chemical environment of the metals in the bulk and on the surface. Experiment conditions used are given in the supplementary information.

2.3 Catalyst testing

Acetone hydrogenation was tested in a fixed-bed at 180°C under 60 bar hydrogen with a flow of 40 ml/min. Prior to reaction, the catalyst was reduced *in situ* at 200°C under 60 bar hydrogen at 100 ml/min. A 0.1 mol/L acetone aqueous solution was fed from the bottom of the reactor at 0.5 ml/min. The liquid products were collected from a 5°C effluent condenser and analyzed with a GC-MS equipped with HP-1701ms column (60×0.32×0.25) and a flame ionization detector. The conversion and selectivity were based on carbon concentrations. For each reaction test, the amount of catalyst was fixed at 30 mg to maintain a constant palladium loading within the reactor.

Additional hydrogenation reactions were performed with propionaldehyde, 2-pentanone, 5-hexen-2-one, benzene, and phenol using the same reactor set-up and GC-MS analysis. However, the reaction conditions for the different molecules were adjusted so as to obtain comparable conversion levels. The reaction conditions for these molecules are given in Table S3.

3. Results and discussion

3.1 Characterization of catalysts

The overall Pd and Fe compositions for the range of catalysts synthesized, as determined by ICP-MS, are given in Table S1. From this measurement, they all had about 0.7 wt% of Pd, so that the reaction results could be compared for equivalent Pd loading. The Pd weight percentage reported corresponds to the mass of Pd divided by the total catalyst mass. Also determined was the Pd molecular percentage, which was defined as the following:

$$\text{Pd mol\%} = \frac{the\ moles\ of\ Pd}{the\ moles\ of\ Pd + the\ moles\ of\ Fe} \times 100\%$$

In addition to the overall metal elemental composition, average elemental compositions for the individual particles was determined using EDS/HAADF-STEM. Table 2 gives the mol% composition measured in the particles as well as the overall concentration in the catalysts. Although the overall Pd composition was in agreement with the nominal composition, the average of the Pd mol% was significantly higher for the measured particles. Therefore, it appeared that the majority of Pd was in contact with Fe within the particles, leaving some of the Fe to form separate iron species with no nearby presence of Pd. HRTEM and EDS images showed homogeneous contrast within the same particle indicating the Pd and Fe were well mixed in each alloy particle, rather than partially segregated. The HRTEM images and detailed elemental concentrations are provided in the supporting information.

Catalyst	Average mol% in Particles [a]	Overall mol% in Catalyst [b]
Pd_{75}	86±18	70
Pd_{45}	85±15	44
Pd_{20}	50±19	16
Pd_{10}	37±17	9

a. determined by EDS and averaged among measured particles; b. determined by ICP

Table 2. Pd concentration in bimetallic catalysts

The Pd dispersion and active surface were measured by CO chemisorption. No background CO adsorption was detected on either the carbon-coated silica support or the supported monometallic Fe, so it was assumed that the chemisorption only occurred on the surface Pd. The Pd dispersion values for the different catalyst are shown in Figure 1. The apparent dispersion of Pd decreased with increasing Fe until reaching a plateau when the Pd mol% reached 45%.

Shown in Figure S1 are representative STEM images for the catalysts and Figure S2 are the corresponding particle size distributions. There were several observations from multiple images for each sample. For Pd_{100}, the particles had a narrow range of particle sizes between 1-2nm. In contrast, the bimetallic catalysts showed a wider range of particle sizes. While particle sizes between 1-2 nm dominated, both smaller particles down to 0.5 nm and larger particles up to 5.5-6 nm were also observed. With increasing Fe content, the fraction of smaller and larger particles increased slightly.

Table 3 gives the calculated metal particle sizes based on surface-averaged diameter, Gauss-averaged diameter, and number-averaged diameter from the STEM images. Since larger particles

have higher weight in calculating surface-averaged diameter than the small particles, the surface-averaged diameters for the bimetallic catalysts were larger than the Gauss-averaged diameters or number-averaged diameters, which was also consistent with the wider range of particle sizes observed for the bimetallic catalysts compared to the monometallic catalyst. The trend for surface-averaged dimeter was also consistent with the trend for metal dispersion as determined by CO chemisorption.

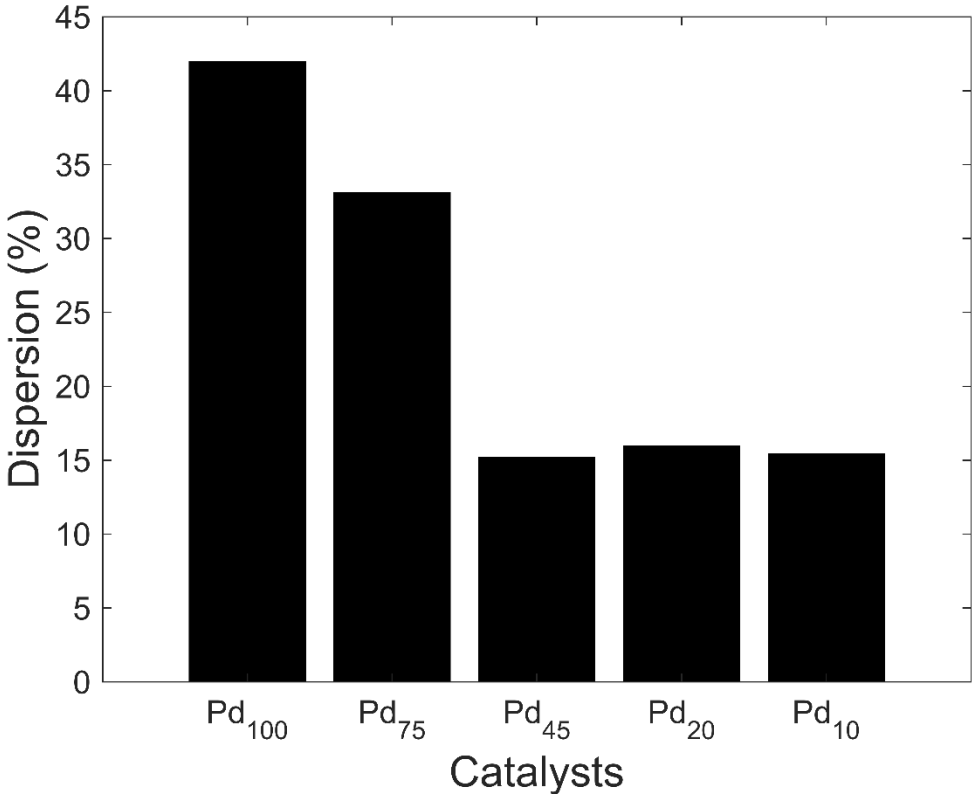

Figure 1. Palladium dispersion from CO chemisorption

Catalyst	**Surface-Averaged Diameter (nm)[a]**	**Gauss-Averaged Diameter (nm)[b]**	**Number-Averaged Diameter (nm)[c]**
Pd_{100}	1.7	1.6	1.6
Pd_{75}	2.1	1.5	1.6
Pd_{45}	3.0	1.1	1.5
Pd_{20}	2.9	1.4	1.8
Pd_{10}	2.7	1.5	1.7

a.Surface-averaged diameter = $\frac{\sum n_i d_i^3}{\sum n_i d_i^2}$, b. Built-in curve fitting function in Origin, c. Number-averaged diameter = $\frac{\sum n_i d_i}{n}$

Table 3. Particle sizes from STEM images

To examine the interaction of the Pd and Fe in the particles, HRTEM was performed. Shown in Figure 2 is a representative image for Pd_{10} where the lattice fringes of 0.202 nm and 0.213 nm corresponded to a metallic Fe phase and an ill-defined Pd-Fe alloy, respectively. A d-spacing of

0.23 nm for metallic Pd(111) has been reported and the incorporation of Fe into the Pd lattice would reduce this value to between 0.20-0.23 nm since an Fe atom is smaller than a Pd atom.[31] Therefore, the existence of the 0.213 nm lattice fringe suggested the existence of a Pd-Fe alloy, i.e., Pd in intimate contact with Fe, which was in agreement with the calculation from elemental analysis. Except for the PdFe alloy, which does not currently have reliable data, the phases were identified using the American Mineralogist Crystal Structure Database. The structures of the metals on the catalysts were evaluated by XRD and XPS as shown in the supporting information for representative samples. No distinguishable peaks were observed for either the Pd or Fe phases, which indicated that the particles were too small for the XRD limit or they were an ill-defined phase found from with the HRTEM images. Similarly, no information was obtained from the XPS results due to the low metal content on the catalysts surface.

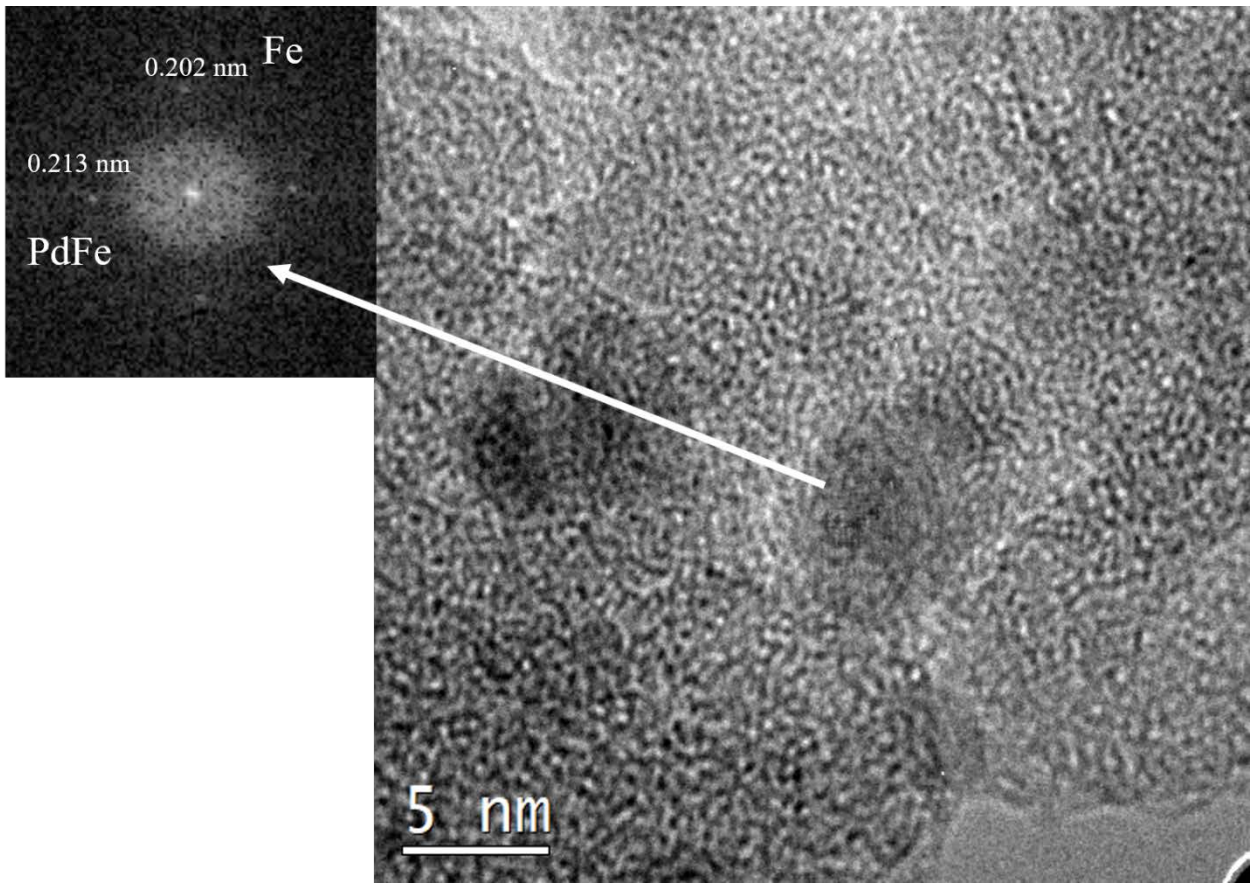

Figure 2. HRTEM image of Pd_{10}

The potential interaction between Pd-Fe was also examined using H_2-TPD of the catalysts as shown in Figure 3. With increasing Fe content, the peak hydrogen desorption temperature increased from 88ºC with Pd_{100} to 194ºC with the iron-rich Pd_{10}, indicating a stronger interaction between Pd and adsorbed hydrogen in the presence of Fe. A reference H_2-TPD on a supported monometallic Fe material gave no adsorption of hydrogen. The difference in interaction strength might be attributable to an electronic density change for the Pd caused by a Pd-Fe interaction. This trend of desorption temperature shift was in agreement with the H_2-TPD of bimetallic Pd-Fe catalyst supported on ordered mesoporous carbon reported by Kim et al.[30] They also performed

XPS analysis of their catalysts, which suggested an electron transfer from Fe to Pd to form a partially negatively charged palladium ($Pd^{\delta-}$). Although CO chemisorption of the current materials gave a similar number of active sites for the Pd_{10}, Pd_{20}, and Pd_{45} catalysts, the H_2-TPD indicated that the binding energy of hydrogen on these sites were different. As such, the surface potential of the sites and their binding energy were different.

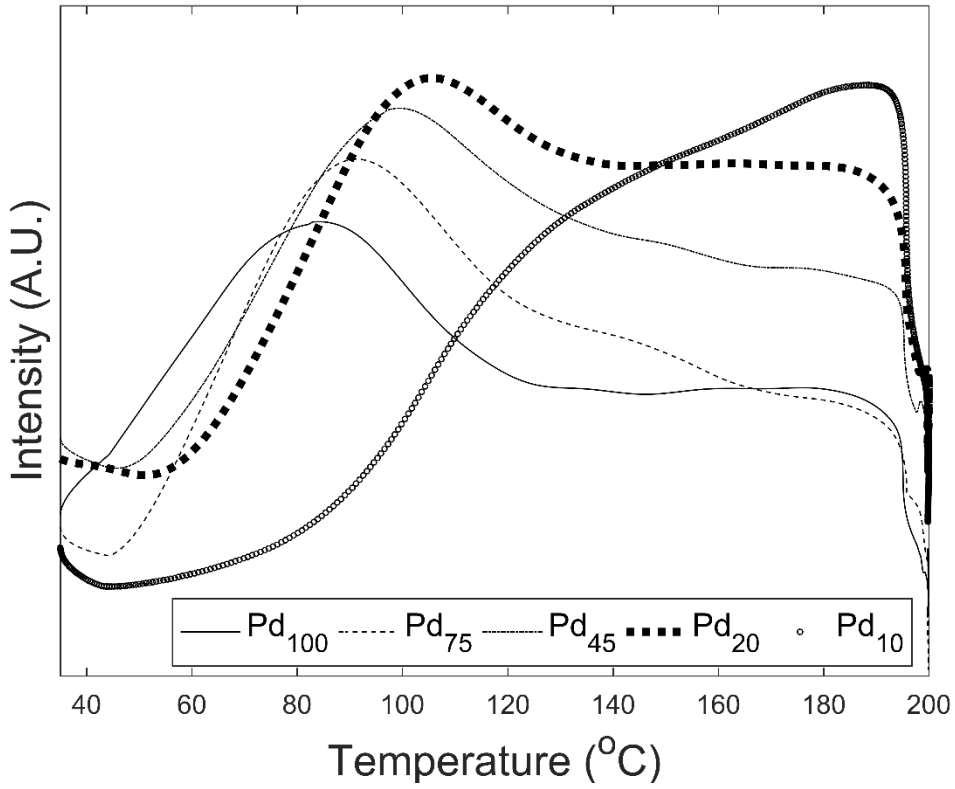

Figure 3. H_2-TPD of the catalysts

3.2 Liquid phase hydrogenation of acetone

For reference, monometallic Fe supported on the carbon-coated silica was screened in the condensed phase acetone hydrogenation reaction. Within the high carbon balances achieved (95-102%) no acetone conversion was observed. This result contrasts with gas-phase acetone hydrogenation reaction results, which gave acetone hydrogenation in a temperature range of 0-98°C[32].This difference in reactivity is likely due to the significant difference in reaction conditions resulting from the gas phase reaction versus the condensed aqueous phase reaction system. Most significantly, Fe remained in its metallic oxidation state in the vapor phase studies, but was likely oxidized in the aqueous phase reaction given its ease of oxidation in water[33,34].

With the Pd containing catalysts, the only product detected in the acetone hydrogenation reaction was isopropanol and the total carbon balance for acetone and isopropanol was >95% for the reaction studies. The <5% carbon loss could be attributed to measurement accuracy limits. The GC analysis was more sensitive to the low concentration compound, so the isopropanol

concentration was more accurate than the acetone concentration for the low conversion studies performed. As such, the isopropanol yield was used for calculation of the apparent turnover frequency (TOF, s^{-1}), which was the amount of isopropanol produced per second per surface palladium atom.

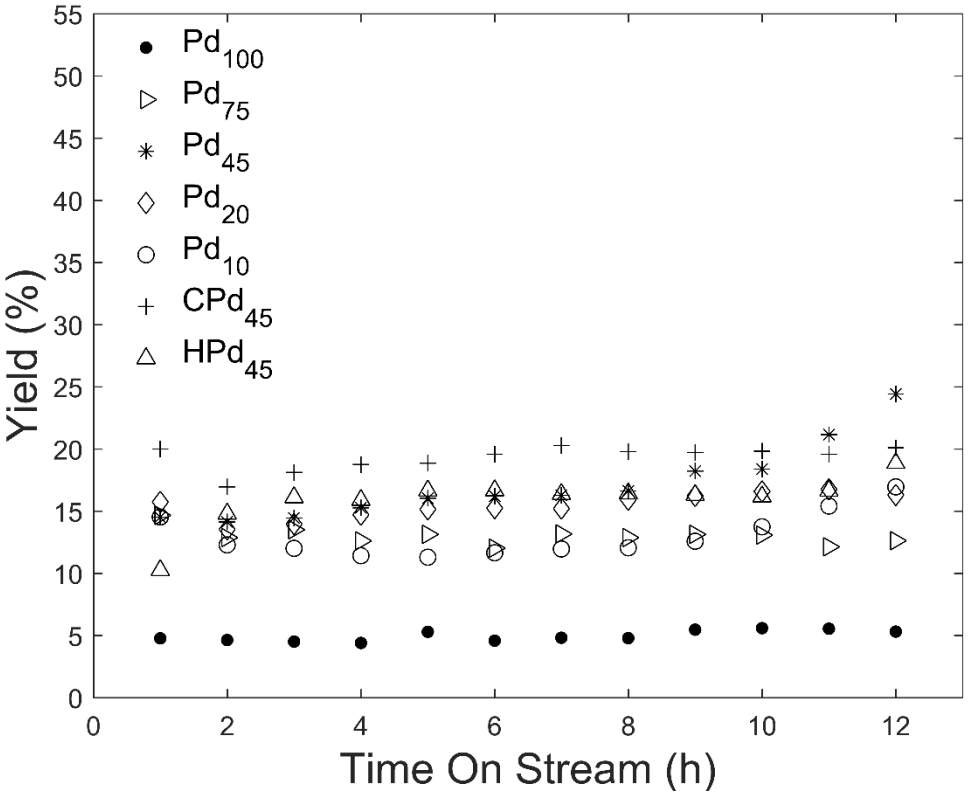

Figure 4 Yield of isopropanol on different catalysts as a function of time-on-stream

The isopropanol yields with the different catalysts are shown in Figure 4. Yields for Pd_{10}, Pd_{20}, Pd_{45} and Pd_{75} were averaged from two replicate runs and the yield values for each run are given in Table S3. Each catalyst showed good reproducibility, especially during the first 8 hours. Therefore, the differences in yield seen for the different catalyst could not be simply attributed to quantification errors. With monometallic Pd, the yield gave a stable value of approximately 5 mol% for 12 hours. The addition of Fe, independently of the amount, at least doubled the yield. While different Fe levels gave relatively similar values, the Fe-rich catalysts (Pd_{10}, Pd_{20}, and Pd_{45}) had higher yields than for the Pd-rich catalyst (Pd_{75}).

Given the multiple synthesis steps for the bimetallic catalysts on carbon-coated silica, variants of the base synthesis condition used for Pd_{45} were also examined. CPd_{45} and HPd_{45} had the same composition, with 1 wt% Pd and a Pd to Fe ratio of 45:55, but they used a different synthesis sequence. CPd_{45} was synthesized by Fe impregnation on silica followed by furfural alcohol impregnation, pyrolysis, and then Pd impregnation. HPd_{45} was synthesized the same way as Pd_{45}, except the Fe precursor was reduced at 200°C in hydrogen before impregnation of the Pd precursor. The variation in performance of these three catalysts was within margin of error for the catalyst testing.

While the incorporation of Fe appeared to enhance the reactivity, it was useful to calculate the TOF for a more direct comparison of the activity of the Pd sites. The number of Pd sites, as determined by CO chemisorption, used for the TOF calculation are given in Table S2. The calculated TOF values are shown in Figure 5 with the baseline Pd_{100} catalyst maintaining a TOF of 0.05 s^{-1} for the 12 h run. Similar to the yield values, the Pd-Fe catalysts all gave higher TOF values than did the Pd_{100} catalyst. However, the TOF results could be placed in three groupings with the lowest value for Pd_{100}, and intermediate value for Pd_{75} and similar higher values for all of the Fe-rich Pd-Fe catalysts. In fact, the TOF values for the Fe-rich catalysts were an order of magnitude larger than that for the Pd_{100} catalyst. The small differences in TOF values between the Fe-rich catalysts were within the experimental error for the study. As the significant yield enhancement was observed for a range of Pd-Fe ratios, the reaction rates were not simply determined by the mass transfer rate, and the TOF difference could not be attributed solely to the differences in active surface area.

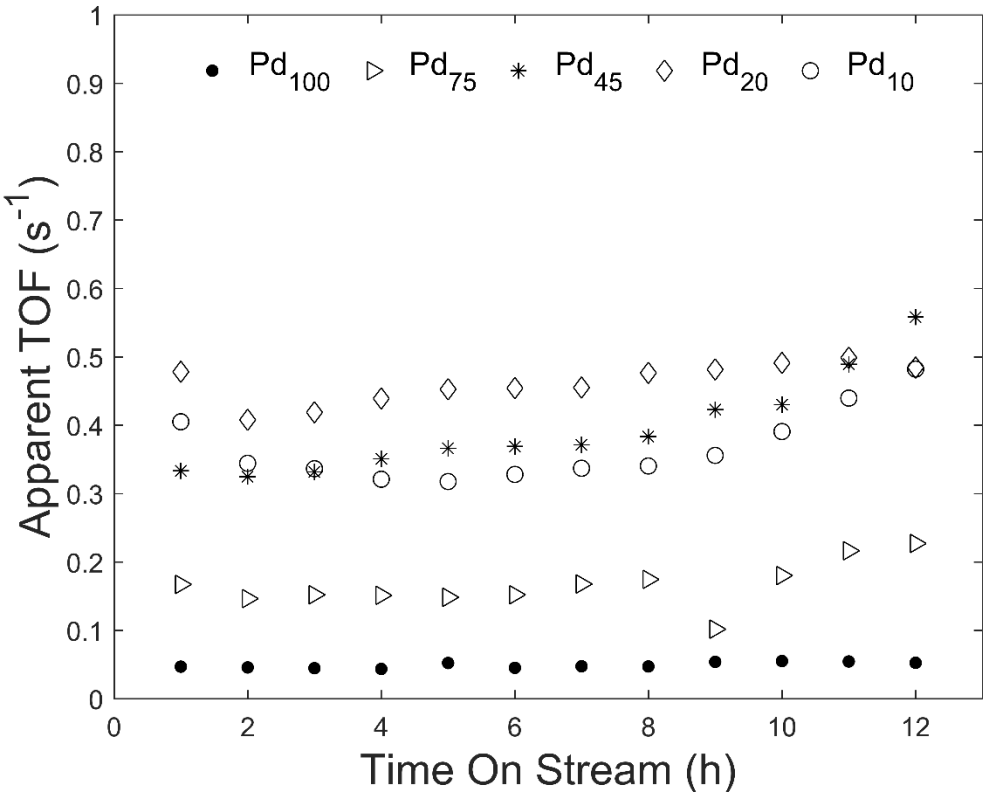

Figure 5. Apparent turnover frequencies (s^{-1}) as a function of time-on-stream

To further probe potential mass transfer limitation, a range of additional rune with the Pd_{100} were performed as summarized in Table S3. By increasing the acetone residence time and H_2 flowrate, the yield of isopropanol increased from approximately 5% to about 32%. As illustrated in the supplementary information, the yield of these two runs roughly matched with the kinetic calculation, indicating that the external mass transfer should not be rate determinative. The existence of internal mass transfer limitation was also evaluated by running the reaction with the Pd_{100} catalyst ground into a finer powder. The powder Pd_{100} yield was approximately the same as

that for the granular Pd_{100} and much smaller than that for the PdFe bimetallic catalysts. Therefore, the reaction on Pd_{100} did not appear to be internal diffusion limited. Although it was possible the more active PdFe bimetallic could have been mass transfer limited, the apparent TOFs on the these catalysts were still an order of magnitude higher than with Pd_{100}, confirming the PdFe bimetallic catalysts were indeed more active than the Pd_{100}.

Taken together the characterization and reaction results suggested that an amorphous Pd-Fe alloy or clusters of intimately mixed Pd and Fe were formed during the synthesis process. While the interactions between the metals were not observed from XRD or XPS, the d-spacing from the HRTEM images as well as the H_2-TPD analysis support their existence. From the Pd-Fe phase diagram[35], Pd between 0-55 mol% in Pd-Fe equilibrium mixtures leads to two stable phases consisting of metallic Fe and Pd_1Fe_1 phase. The HRTEM results were consistent with these phases as particles were found to contain well mixed Fe and Pd_1Fe_1 phase. As the Pd content was held fixed for all of the catalysts, the amount of the Pd_1Fe_1 phase in the Fe-rich catalysts (Pd_{10}, Pd_{20}, and Pd_{45}) would be the same if that alloy was formed. While the characterization results did not provide direct evidence of an equivalent amount of the Pd_1Fe_1 phase for these catalysts, they did have the same amount of active surface area as measured from CO chemisorption. For the higher Pd content, the Pd-Fe phase diagram[35] shows that a Pd_3Fe_1 phase could be formed instead of Pd_1Fe_1. Therefore, it is possible that the lower TOF associated with Pd_{75} relative to Pd_{10}, Pd_{20}, and Pd_{45} could be related to the existence of different Pd-Fe phases.

The Fe in the Pd-Fe alloy may have altered the electron density of the Pd thereby modifying the activity of the Pd sites. A Pd-Fe alloy, as reported previously[30,36], can lead to a partially negatively charged Pd, described as $Pd^{\delta-}$. In the metallic state, Pd^0 bonds with C=O through a σ-bond with the carbon and back donation of electrons from the filled Pd π-orbitals to the empty oxygen orbitals[37]. If the adsorption of the C=O moiety is the rate limiting step in the hydrogenation reaction, it is possible that the presence of $Pd^{\delta-}$ reduced the adsorption energy by forming a stronger attractive force with $C^{\delta+}$. Given the higher electron density of $Pd^{\delta-}$, the energy of the O-π-bond-$Pd^{\delta-}$ could be higher than that of the O-π-bond-Pd, which would mean the activation energy for hydrogen addition on carbonyl would be lower leading to a higher overall reaction rate.

While the potential alloying effect in Pd-Fe catalysts was consistent with the reaction results, the complexity of bimetallic catalysts requires evaluation of additional factors that could have contributed to the different catalytic performance compared to the monometallic counterpart, such as particle size effects, alteration of reactant adsorption, and hydrogen availability due to a spillover effect. These possible effects were each examined from the characterization and reaction results.

The TEM images showed that the number-averaged particle sizes for the Pd and bimetallic Pd-Fe catalysts were similar. However, a particle size effect could not be definitively excluded, since metallic Fe and the Pd-Fe alloy were well mixed in the same particle. It was reported that on Fe_2O_3 supports, Pd formed smaller islands[31]. Therefore, it is possible that in the bimetallic catalysts the Pd-Fe alloy was segregated by the metallic Fe forming smaller clusters. However, this should have been accounted for in the CO chemisorption characterization.

In addition to affecting the reaction through Pd modification, Fe could also affect the reaction more directly by adsorbing oxygen through the C=O group, since Fe is an oxophilic metal. This assisted adsorption by Fe has been proposed to explain the increased selectivity of C-O bond cleavage in gas-phase hydrogenolysis reactions[14,30]. However, this factor relates to oxygen adsorption on metallic Fe, which likely does not exist with the current aqueous phase conditions. Phua et al.[33] and Stein et al.[34] reported significant deactivation of iron catalysts upon oxidation by water. Although multiple groups observed increased reducibility of Fe species in the presence of Pd[19,38], Kim et al.[30] examined the temperature programed reduction of Pd-Fe bimetallics supported on ordered mesoporous carbon and found the lowest reduction temperature to be 239°C, which is higher than either the reduction temperature or reaction temperature used here.

Hydrogen spillover enhancement due to the presence of Fe was likely not a factor for the increased reaction rate because the reaction rate did not continue to increase as Fe loading increased. If the enhanced reaction rate was primarily caused by a hydrogen spillover effect, both the product yield and TOF would be expected to increase with Fe loading, since increased Fe content would provide more sites for adsorbed hydrogen leading to higher hydrogen coverage and apparent reaction rates. The potential for enhanced hydrogen adsorption rate with lower activation energy will be subsequently discussed below in the liquid phase hydrogenation of other molecules, but the results suggested that Fe addition impacted hydrogen adsorption.

While still a postulate, the experimental results suggested that it is the $Pd^{\delta-}$ in Pd-Fe alloys that was the primary effect for the enhanced reaction rate upon Fe addition. Since the elemental analysis showed that the majority of the Pd was in close contact with Fe, the active surface area quantified by CO chemisorption represented the alloyed Pd surface very well. The similar values of the active surface area for the Pd_{45}, Pd_{20}, Pd_{10} (Table S2) was in good agreement with the postulate.

3.3 Liquid phase hydrogenation of other molecules

To further explore the impact of Fe addition to Pd catalysts in condensed phase reaction systems the hydrogenation of 2-pentanone, propionaldehyde, 5-hexen-2-one, benzene and phenol were also performed. Unfortunately, several of these molecules did not have selective conversion to a single hydrogenation product as was the case with acetone to isopropanol. As such, an apparent TOF was calculated based on the molar rate of consumption of the reactant per mole of active sites. Additionally, a TOF_{H_2} was calculated using the following equation:

$$TOF_{H_2} = \frac{consumption\ rate\ of\ H_2}{mole\ of\ active\ sites}$$

where the consumption rate of H_2 was calculated from the production rate of all hydrogenation products. As the TOF_{H_2} is based on the formation of hydrogenated products, it is specifically a measurement of the hydrogenation activity. It should be noted that both the apparent TOF and the TOF_{H_2} have the same values for acetone hydrogenation as the TOF discussed previously results from a reaction only yielding a single product.

3.3.1 Hydrogenation of carbonyl groups

Figure 6 shows the comparison of the apparent TOF values for 2-pentanone, and propionaldehyde. The conversion and selectivity values are given in Table S5. Similar to acetone hydrogenation, the bimetallic catalysts also showed a significantly higher activity than with the monometallic catalyst, although the activity did appear to decrease somewhat as the Fe content increased. The apparent TOFs for monometallic Pd_{100} were similar for all of the carbonyl containing species acetone, 2-pentanone, and propionaldehyde ($0.05s^{-1}$, $0.04\ s^{-1}$, and $0.04\ s^{-1}$, respectively), suggesting the mechanism for converting the carbonyl group in these molecules proceeds through a similar mechanism. In contrast, the magnitude of rate enhancement with Fe content differs suggesting that this rate enhancement was related to the reactant rather than hydrogen.

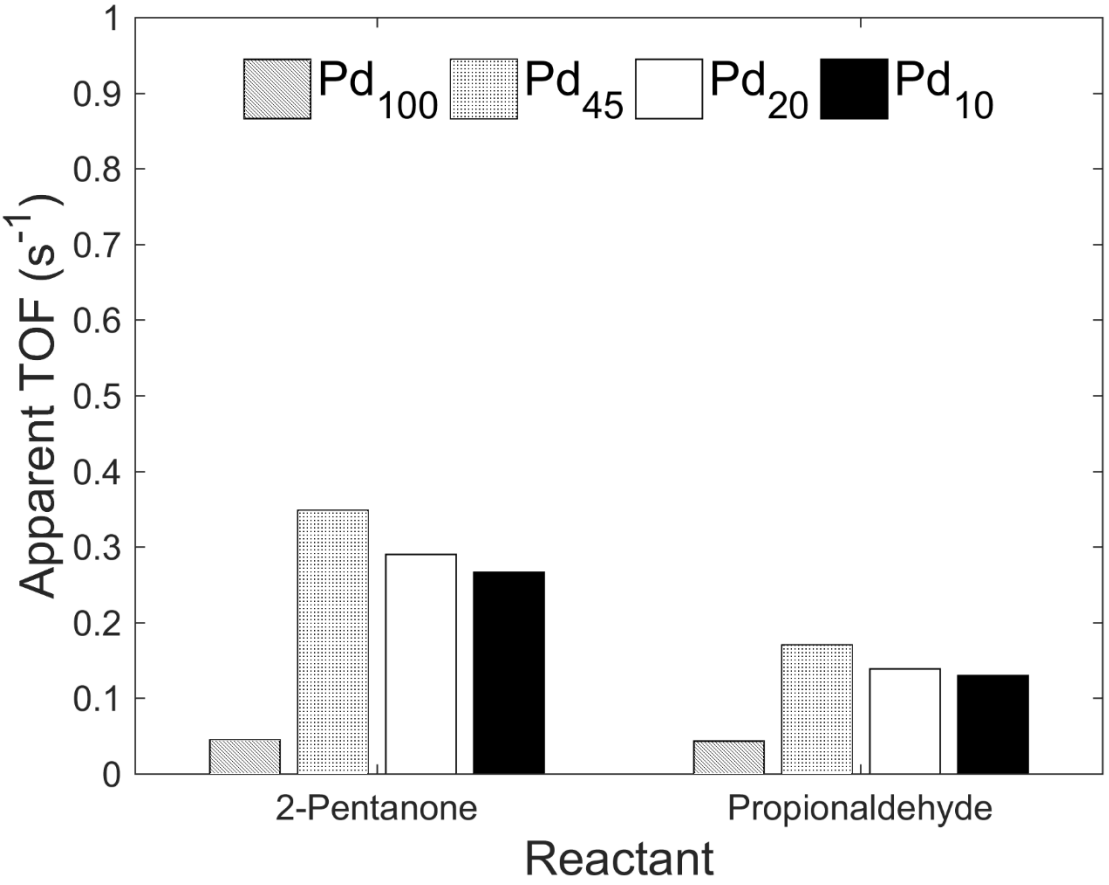

Figure 6. Apparent TOFs of hydrogenation for 2-pentanone and propionaldehyde hydrogenation

The products in the propionaldehyde reaction included 1-propanol, 2-methyl-pentanal, and 2-methyl-pentanol. Therefore, to compare the propionaldehyde hydrogenation activity of the catalysts the TOF_{H_2} values were also calculated. Table 5 compares the apparent TOF and TOF_{H_2} values for the reaction. Given the definitions for these two values, the ratio of TOF_{H_2} and apparent TOF effectively provides the hydrogenation product selectivity. Since the conversions with the PdFe bimetallic catalysts were considerably higher than with Pd_{100}, and the TOFs for 2-pentanone and propionaldehyde were both lower than for acetone, any mass transder limitation would be in the opposite direction of the observed activity enhancement. The low carbon

balance for the Pd_{100} was likely due to the decarbonylation reaction leading to gaseous products. As shown in the table, Fe addition specifically enhanced the hydrogenation rate as the selectivity to the hydrogenation products was significantly increased. The hydrogenation selectivity enhancement for propionaldehyde suggested that the rate limiting step was hydrogenation of the adsorbed reactant, which would be consistent with the $Pd^{\delta-}$ postulate discussed above.

Liao et al.[36] synthesized Pd-Fe bimetallics on Fe_2O_3. They reported, based on XPS and EXAFS results, that the electron density of Pd had a reverse trend with the number of neighboring Fe atoms. As the amount of Fe in the catalysts increased, the electron density of the Pd increased, leading to a higher H_2 desorption temperature in TPD analysis, which agreed with our H_2-TPD results. The electron density dependency on the local Pd-Fe ratio could explain the activity differences observed for 2-pentanol and propionaldehyde hydrogenation.

Catalyst	**TOF(s^{-1})**	**TOF_{H_2} (s^{-1})**	**Hydrogenation Selectivity**	**Carbon Balance**
Pd_{100}	0.043	0.024	56%	77%
Pd_{45}	0.17	0.165	96%	97%
Pd_{20}	0.139	0.118	85%	90%
Pd_{10}	0.13	0.104	80%	87%

Table 5. Reaction results for propionaldehyde hydrogenation

3.3.2 Hydrogenation of 5-hexen-2-one, benzene and phenol

The next set of molecules tested were selected to examine the impact of Fe addition on the hydrogenation of unsaturated carbon-carbon bonds in the condensed phase. To focus on the reactivity of its unsaturated carbon-carbon double bond, 5-hexen-2-one was tested at 40°C, which was too low of a temperature for hydrogenation of the carbonyl bond.

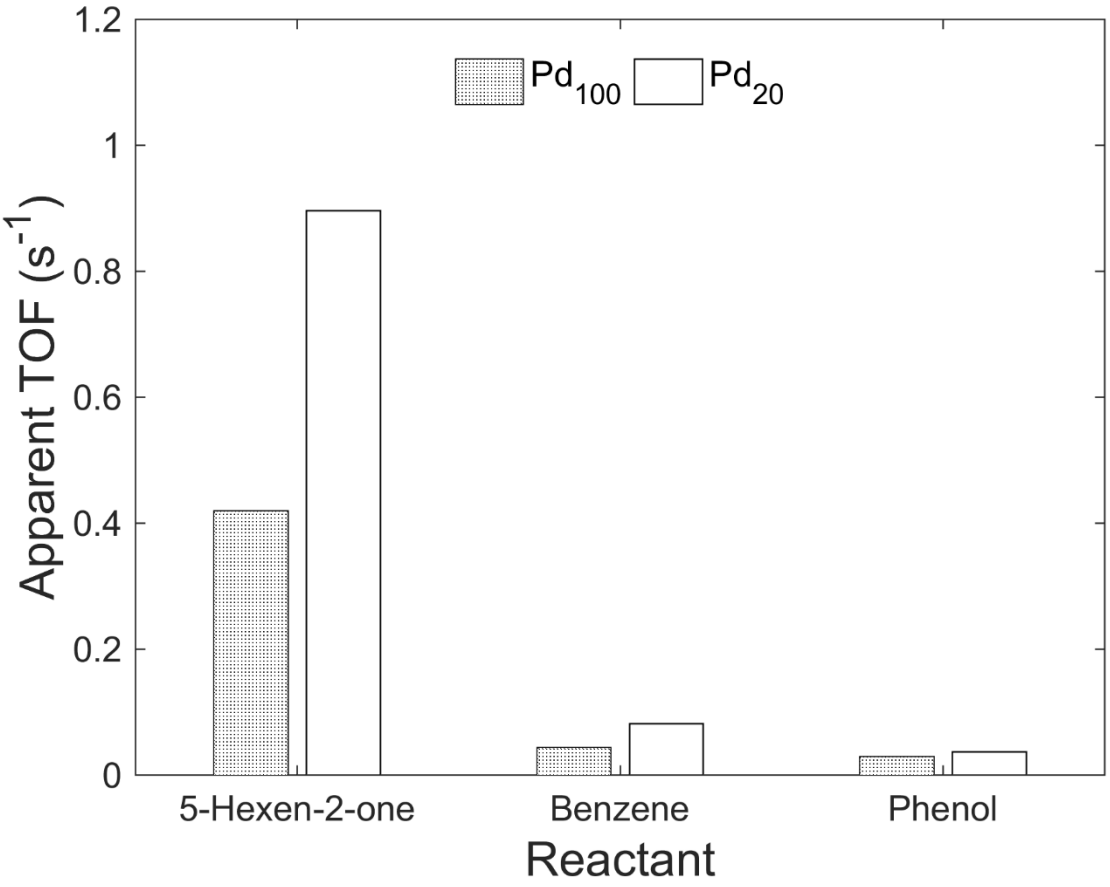

Figure 7. Apparent TOFs for 5-hexen-2-one, benzene and phenol hydrogenation

Figure 7 compares the apparent TOFs for 5-hexen-2-one, benzene and phenol based on the consumption rate of the reactants. As seen in Table S6, Pd_{100} had a considerably higher conversion than with Pd_{20} for all three of the molecules, indicating that mass transfer limitation did not dictate the rates of the reactions. As with the carbonyl hydrogenation, the apparent TOFs for the C=C bond and aromatic rings increased with Fe inclusion, but to a significantly lower degree than for the C=O group with the previous reactants. The apparent TOFs for 5-hexen-2-one and benzene with Pd_{20} were about twice that with Pd_{100}, whereas the apparent TOF for phenol with Pd_{20} was only marginally higher than with Pd_{100}. However, the product selectivity for both 5-hexen-2-one and phenol changed. The reaction products from 5-hexen-2-one hydrogenation included 2-hexanone, and isomers, 3-hexen-2-one and 4-hexen-2-one. For phenol with Pd_{100}, the selectivity for cyclohexanone and cyclohexanol was 81.4 mol% and 18.6 mol%, respectively, while the values were 25.5 mol% and 74.5 mol% on Pd_{20}. The only product detected from benzene hydrogenation was cyclohexane for both Pd_{100} and Pd_{20}. For direct comparison of the hydrogenation activity, TOF_{H_2} values were also calculated for 5-hexane-2-one, benzene and phenol as given in Table 6.

Reactant \ Catalyst	Pd_{100}	Pd_{20}	$\mathbf{TOF_{H_2}}$ on Pd_{20}/ $\mathbf{TOF_{H_2}}$ on Pd_{100}	Reaction Temperature(°C)
Propionaldehyde	0.024	0.118	4.9	180
5-Hexen-2-one	0.349	0.739	2.1	40
Benzene	0.106	0.230	2.2	180
Phenol	0.064	0.100	1.6	180

Table 6. TOF_{H_2}(s^{-1}) values for the hydrogenation reactions

It is commonly accepted that the reactivity of functional groups towards catalytic hydrogenation follows the order of C=C > aldehyde > aromatics, which was the same trend observed in the current work as seen clearly in the high TOF_{H_2} of 5-hexen-2-one even when the reaction temperature was lower than in the other reactions. As the C=C and aromatic bonds are not oxygen-containing, the higher apparent TOFs for the bimetallic catalysts could not be attributed to the adsorption of oxygen on oxophilic iron, which further supported the postulate that the enhanced activity for C=O hydrogenation needed to be attributed to other reasons.

The adsorption of C=C moieties on Pd surfaces is often described as having a π-character[37], which would be expected to have inhibition by repulsion between the C=C and $Pd^{\delta-}$. However, this repulsion could also weaken the adsorption strength of the C=C on Pd surface, which could facilitate the surface reaction rate as suggested by mechanistic studies in the system reported by Katano et al.[39] and Ohno et al.[40] for 1,3-butadiene and 2-butene, respectively. They each reported in their reaction systems that several adsorbed species with different adsorption energies were present the on Pd surface. They proposed the weakest bonded species desorbed, the moderate bonded species hydrogenated, and the strongly bonded species stayed on the surface and decomposed leading to catalyst deactivation. By analogy, it is possible that the existence of the $Pd^{\delta-}$ increased the number of moderate bonded species. Similarly, the gas-phase hydrogenation of benzene on Pd studies suggested the rate-limiting step for benzene hydrogenation is the sequential hydrogen addition to the adsorbed reactant, which is in competition with decomposition and coke[41]. The doubled TOF_{H_2} value found here for benzene would be consistent with the postulate that $Pd^{\delta-}$ accelerates the surface reaction.

In previous studies of phenol hydrogenation on Pd the reaction sequence proposed is shown in Figure 8[4,42,43]. For this sequence, the aromatic ring is first partially hydrogenated with hydrogen, forming 1-cyclohexen-1-ol, which then isomerizes to cyclohexanone instantaneously in step 2 yielding a carbonyl group that is hydrogenated to a hydroxyl group in the final step. In agreement with the facilitated hydrogenation rate of the carbonyl group observed with Pd_{20}, the improved selectivity to the full phenol hydrogenation product was consistent with the Pd-Fe catalysts enhancing hydrogenation of the carbonyl bonds to a greater extent than the hydrogenation of C=C and aromatic bonds.

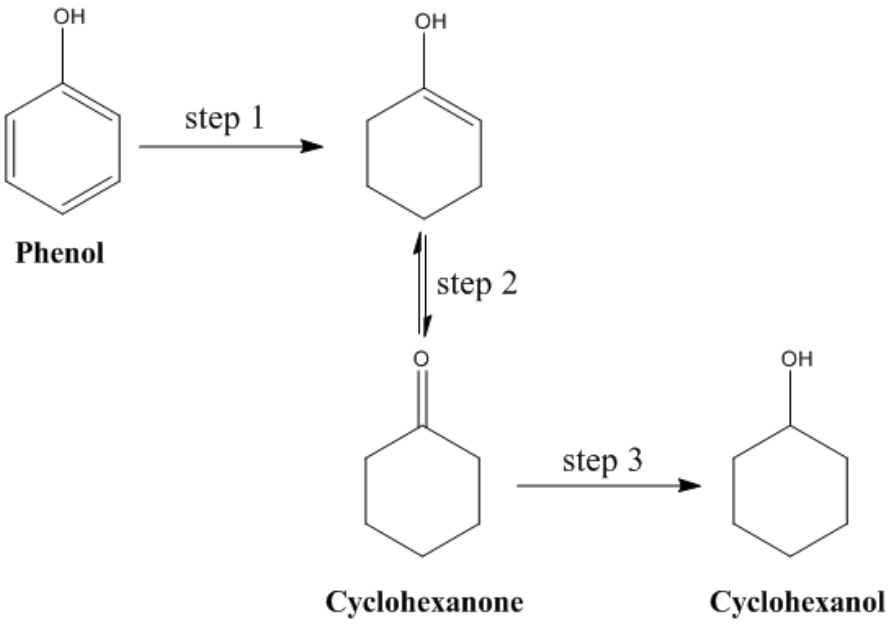

Figure 8. Proposed hydrogenation route for phenol

It has been established that saturated aldehydes and ketones can isomerize to an enol, forming a carbon-carbon double bond and an adjacent hydroxyl group[44]. As observed for 5-hexen-2-one hydrogenation, the C=C hydrogenation rate was increased less than that of C=O, so the smaller increase in TOF_{H_2} value with Pd_{20} was likely due to a smaller increase in hydrogenation rate for the enols (allyl alcohol for propionaldehyde and 3-pentan-2-ol for 2-pentanol). Taken together, the significant increase in carbonyl hydrogenation rate and modest increase in C=C hydrogenation rate would be expected to result in an overall TOF_{H_2} enhancement for propionaldehyde and 2-pentanone between that for acetone and the C=C bond, which was consistent with the observation in this study.

4. Conclusion

Bimetallic Pd-Fe catalysts were found to have significantly increased TOFs for the condensed-phase hydrogenation of carbonyl, C=C and aromatics compared to monometallic Pd catalyst. The extent of the activity enhancement varied by the moiety being hydrogenated as well as the Pd-to-Fe ratio. The optimal Pd-to-Fe ratio appeared to be 45 mol% of Fe relative to Pd. The increased activity of the bimetallic catalysts relative to the monometallic catalyst was proposed to be due to modification of the Pd by Fe leading to formation of $Pd^{\delta-}$, as Fe was found to have no reactivity under the reaction conditions used. An important basis for this postulate was the much greater increase in carbonyl hydrogenation activity than for C=C and aromatic hydrogenation, which would be consistent with the formation of a $Pd^{\delta-}$ species. Unfortunately, the low metal loadings used in the catalysts limited direct observation of this proposed species, but HRTEM and CO chemisorption analyses supported the reaction results.

Acknowledgement

We appreciate the help of Dr. Dapeng Jing for XPS analysis, Dr. Patrick Johnston for ICP analysis, and Dr. Scott Schlorholtz and David Kuhn for XRD analysis. We would also like to thank Professor Jean-Philippe Tessonnier for helpful discussions. This work was supported by the National Science Foundation Center for Biorenewable Chemicals [EEC-0813570].

References

[1] M. Besson, P. Gallezot, C. Pinel, Conversion of biomass into chemicals over metal catalysts, Chem. Rev. 114 (2014) 1827–1870. doi:10.1021/cr4002269.

[2] B. Roldan Cuenya, F. Behafarid, Nanocatalysis: Size- and shape-dependent chemisorption and catalytic reactivity, Surf. Sci. Rep. 70 (2015) 135–187. doi:10.1016/j.surfrep.2015.01.001.

[3] O.M. Wilson, M.R. Knecht, J.C. Garcia-Martinez, R.M. Crooks, Effect of Pd nanoparticle size on the catalytic hydrogenation of allyl alcohol, J. Am. Chem. Soc. 128 (2006) 4510–4511. doi:10.1021/ja058217m.

[4] Y. Wang, J. Yao, H. Li, D. Su, M. Antonietti, Highly selective hydrogenation of phenol and derivatives over a pd@carbon nitride catalyst in aqueous media, J. Am. Chem. Soc. 133 (2011) 2362–2365. doi:10.1021/ja109856y.

[5] Y.S. Yun, H. Park, D. Yun, C.K. Song, T.Y. Kim, K.R. Lee, Y. Kim, J.W. Han, J. Yi, Tuning the electronic state of metal/graphene catalysts for the control of catalytic activity: Via N- and B-doping into graphene, Chem. Commun. 54 (2018) 7147–7150. doi:10.1039/c8cc03107j.

[6] L.M. Falicov, G.A. Somorjai, Correlation between Catalytic Activity and Bonding and Coordination Number of Atoms and Molecules on Transition Metal Surfaces : Theory and Experimental Evidence Author (s): L . M . Falicov and G . A . Somorjai Source : Proceedings of the National Acade, Proc. Natl. Acad. Sci. 82 (1985) 2207–2211.

[7] Y. Mei, Y. Lu, F. Polzer, M. Ballauff, M. Drechsler, Catalytic activity of palladium nanoparticles encapsulated in spherical poly electrolyte brushes and core-shell microgels, Chem. Mater. 19 (2007) 1062–1069. doi:10.1021/cm062554s.

[8] M.A. Kulagina, P.A. Simonov, E.Y. Gerasimov, R.I. Kvon, A. V. Romanenko, To the nature of the support effect in palladium-catalyzed aqueous-phase hydrogenation of maleic acid, Colloids Surfaces A Physicochem. Eng. Asp. 526 (2017) 29–39. doi:10.1016/j.colsurfa.2016.11.037.

[9] U.K. Singh, M.A. Vannice, Kinetics of liquid-phase hydrogenation reactions over supported metal catalysts - A review, Appl. Catal. A Gen. 213 (2001) 1–24. doi:10.1016/S0926-860X(00)00885-1.

[10] P. Mäki-Arvela, J. Hájek, T. Salmi, D.Y. Murzin, Chemoselective hydrogenation of carbonyl compounds over heterogeneous catalysts, Appl. Catal. A Gen. 292 (2005) 1–49. doi:10.1016/j.apcata.2005.05.045.

[11] M. Sankar, N. Dimitratos, P.J. Miedziak, P.P. Wells, C.J. Kiely, G.J. Hutchings, Designing bimetallic catalysts for a green and sustainable future, Chem. Soc. Rev. 41 (2012) 8099–8139. doi:10.1039/c2cs35296f.

[12] C. Espro, B. Gumina, E. Paone, F. Mauriello, Upgrading Lignocellulosic Biomasses: Hydrogenolysis of Platform Derived Molecules Promoted by Heterogeneous Pd-Fe Catalysts, Catalysts. 7 (2017) 78. doi:10.3390/catal7030078.

[13] B. Han, C. Xu, Nanoporous PdFe alloy as highly active and durable electrocatalyst for oxygen reduction reaction, Int. J. Hydrogen Energy. 39 (2014) 18247–18255. doi:10.1016/j.ijhydene.2014.09.006.

[14] E. Paone, C. Espro, R. Pietropaolo, F. Mauriello, Selective arene production from transfer hydrogenolysis of benzyl phenyl ether promoted by a co-precipitated Pd/Fe3O4 catalyst, Catal. Sci. Technol. 6 (2016) 7937–7941. doi:10.1039/c6cy01626j.

[15] G.W. Huber, J.W. Shabaker, S.T. Evans, J.A. Dumesic, Aqueous-phase reforming of ethylene glycol over supported Pt and Pd bimetallic catalysts, Appl. Catal. B Environ. 62 (2006) 226–235. doi:10.1016/j.apcatb.2005.07.010.

[16] Y. Tang, S. Cao, Y. Chen, T. Lu, Y. Zhou, L. Lu, J. Bao, Effect of Fe state on electrocatalytic activity of Pd-Fe/C catalyst for oxygen reduction, Appl. Surf. Sci. 256 (2010) 4196–4200. doi:10.1016/j.apsusc.2010.01.124.

[17] X. Wang, R.J. Gorte, The effect of Fe and other promoters on the activity of Pd/ceria for the water-gas shift reaction, Appl. Catal. A Gen. 247 (2003) 157–162. doi:10.1016/S0926-860X(03)00095-4.

[18] Ö. Metin, A. Mendoza-Garcia, D. Dalmizrak, M.S. Gültekin, S. Sun, FePd alloy nanoparticles assembled on reduced graphene oxide as a catalyst for selective transfer hydrogenation of nitroarenes to anilines using ammonia borane as a hydrogen source, Catal. Sci. Technol. 6 (2016) 6137–6143. doi:10.1039/c6cy00118a.

[19] F. Pinna, M. Selva, M. Signoretto, G. Strukul, F. Boccuzzi, A. Benedetti, P. Canton, G. Fagherazzi, Pd-Fe/SiO2 Catalysts in the Hydrogenation of 2,4-Dinitrotoluene, J. Catal. 150 (1994) 356–367.

[20] N. Lingaiah, P.S. Sai Prasad, P.K. Rao, L.E. Smart, F.J. Berry, Studies on magnesia supported mono- and bimetallic Pd-Fe catalysts prepared by microwave irradiation method, Appl. Catal. A Gen. 213 (2001) 189–196. doi:10.1016/S0926-860X(00)00888-7.

[21] E. V. Golubina, E.S. Lokteva, V. V. Lunin, N.S. Telegina, A.Y. Stakheev, P. Tundo, The role of Fe addition on the activity of Pd-containing catalysts in multiphase hydrodechlorination, Appl. Catal. A Gen. 302 (2006) 32–41. doi:10.1016/j.apcata.2005.12.020.

[22] J. Lee, Y.T. Kim, G.W. Huber, Aqueous-phase hydrogenation and hydrodeoxygenation of biomass-derived oxygenates with bimetallic catalysts, Green Chem. 16 (2014) 708–718. doi:10.1039/c3gc41071d.

[23] M.G. Musolino, C. Busacca, F. Mauriello, R. Pietropaolo, Aliphatic carbonyl reduction promoted by palladium catalysts under mild conditions, Appl. Catal. A Gen. 379 (2010) 77–86. doi:10.1016/j.apcata.2010.03.008.

[24] V.I. Pârvulescu, G. Filoti, V. Pârvulescu, N. Grecu, E. Angelescu, I. V. Nicolescu, Styrene hydrogenation on supported Pd, Fe and Pd-Fe/γ-Al 2 O 3 catalysts, J. Mol. Catal. 89 (1994) 267–282. doi:10.1016/0304-5102(93)E0312-5.

[25] A. Fukuoka, T. Kimura, M. Ichikawa, Selective Hydrogenation of CO into C1 and C2 Alcohols by SiO2-supported RhFe, PtFe, and PdFe Bimetallic Cluster-derived Catalysts, J. Chem. Soc. Chem. Commun. (1988) 428–430.

[26] J. Morales, R. Hutcheson, C. Noradoun, I.F. Cheng, Hydrogenation of phenol by the Pd/Mg and Pd/Fe bimetallic systems under mild reaction conditions, Ind. Eng. Chem. Res. 41 (2002) 3071–3074. doi:10.1021/ie0200510.

[27] H. Tamai, Y. Kataoka, F. Nishiyama, H. Yasuda, Characteristics and catalytic activity of carbons obtained from pitch containing noble metal complexes, Carbon N. Y. 38 (2000) 899–906. doi:10.1016/S0008-6223(99)00186-4.

[28] E.M. Crabb, R. Marshall, Properties of alumina supported Pd-Fe and Pt-Fe catalysts prepared using surface organometallic chemistry, Appl. Catal. A Gen. 217 (2001) 41–53. doi:10.1016/S0926-860X(01)00578-6.

[29] T. Yuan, W.D. Marshall, Catalytic hydrogenation of polyaromatic hydrocarbon (PAH) compounds in supercritical carbon dioxide over supported palladium, J. Environ. Monit. 9 (2007) 1344–1351. doi:10.1039/b715318j.

[30] J.K. Kim, J.K. Lee, K.H. Kang, J.C. Song, I.K. Song, Selective cleavage of C-O bond in benzyl phenyl ether to aromatics over Pd-Fe bimetallic catalyst supported on ordered mesoporous carbon, Appl. Catal. A Gen. 498 (2015) 142–149. doi:10.1016/j.apcata.2015.03.034.

[31] A. Mansouri, N. Semagina, Palladium islands on iron oxide nanoparticles for hydrodesulfurization catalysis, Catal. Sci. Technol. 8 (2018) 2323–2332. doi:10.1039/c8cy00088c.

[32] C.T.H. Stoddart, C. Kemball, The catalytic hydrogenation of acetone on evaporated metallic films, J. Colloid Sci. 11 (1956) 532–542. doi:10.1016/0095-8522(56)90169-6.

[33] P.H. Phua, L. Lefort, J.A.F. Boogers, M. Tristany, J.G. De Vries, Soluble iron nanoparticles as cheap and environmentally benign alkene and alkyne hydrogenation catalysts, Chem. Commun. (2009) 3747–3749. doi:10.1039/b820048c.

[34] M. Stein, J. Wieland, P. Steurer, F. Tölle, R. Mülhaupt, B. Breit, Iron nanoparticles supported on chemically-derived graphene: Catalytic hydrogenation with magnetic catalyst separation, Adv. Synth. Catal. 353 (2011) 523–527. doi:10.1002/adsc.201000877.

[35] T.B. Massalski, J.L. Murry, L.H. Bennett, H. Baker, Binary alloy phase diagrams, 1st ed., American Society for Metals, Metals Park, Ohio, 1986.

[36] F. Liao, T.W.B. Lo, D. Sexton, J. Qu, C.T. Wu, S.C.E. Tsang, PdFe nanoparticles as selective catalysts for C-C cleavage in hydrogenolysis of vicinal diol units in biomass-derived chemicals, Catal. Sci. Technol. 5 (2015) 887–896. doi:10.1039/c4cy01159g.

[37] V. Ponec, G.C. Bond, Catalysis by Metals and Alloys, Elsevier Science B.V, The Netherlands, 1995.

[38] A.J.R. Hensley, Y. Hong, R. Zhang, H. Zhang, J. Sun, Y. Wang, J.S. McEwen, Enhanced Fe2O3 reducibility via surface modification with Pd: Characterizing the synergy within Pd/Fe catalysts for hydrodeoxygenation reactions, ACS Catal. 4 (2014) 3381–3392. doi:10.1021/cs500565e.

[39] S. Katano, H.S. Kato, M. Kawai, K. Domen, Selective partial hydrogenation of 1,3-butadiene to butene on Pd(110): Specification of reactant adsorption states and product stability, J. Phys. Chem. B. 107 (2003) 4–7. doi:10.1021/jp022410a.

[40] S. Ohno, M. Wilde, K. Mukai, J. Yoshinobu, K. Fukutani, Mechanism of Olefin Hydrogenation Catalysis Driven by Palladium-Dissolved Hydrogen, J. Phys. Chem. C. 120 (2016) 11481–11489. doi:10.1021/acs.jpcc.6b00987.

[41] P. Chou, M.A. Vannice, Benzene hydrogenation over supported and unsupported palladium. I. Kinetic behavior, J. Catal. 107 (1987) 129–139. doi:10.1016/0021-9517(87)90278-8.

[42] G. Neri, A.M. Visco, A. Donato, C. Milone, M. Malentacchi, G. Gubitosa, Hydrogenation of

phenol to cyclohexanone over palladium and alkali-doped palladium catalysts, Appl. Catal. A, Gen. 110 (1994) 49–59. doi:10.1016/0926-860X(94)80104-5.

[43] J. Chen, W. Zhang, L. Chen, L. Ma, H. Gao, T. Wang, Direct selective hydrogenation of phenol and derivatives over polyaniline-functionalized carbon-nanotube-supported palladium, Chempluschem. 78 (2013) 142–148. doi:10.1002/cplu.201200276.

[44] S. Tuokko, K. Honkala, P.M. Pihko, Pd/C-Catalyzed Hydrosilylation of Enals and Enones with Triethylsilane: Conformer Populations Control the Stereoselectivity, ACS Catal. 7 (2017) 480–493. doi:10.1021/acscatal.6b02856.